



Short communication

Toxicological and pharmacological evaluation, antioxidant, ADMET and molecular modeling of selected racemic chromenotacrines {11-amino-12-aryl-8,9,10,12-tetrahydro-7H-chromeno[2,3-b]quinolin-3-ols} for the potential prevention and treatment of Alzheimer's disease



María Jesús Oset-Gasque^{a,b,*}, María Pilar González^a, Javier Pérez-Peña^a,
Nuria García-Font^a, Alejandro Romero^c, Javier del Pino^c, Eva Ramos^c,
Dimitra Hadjipavlou-Litina^d, Elena Soriano^e, Mourad Chioua^f, Abdelouahid Samadi^f,
Dushyant S. Raghuvanshi^g, Krishna N. Singh^{g,***}, José Marco-Contelles^{f,b,**}

^a Departamento de Bioquímica y Biología Molecular II, Facultad de Farmacia, Universidad Complutense de Madrid (UCM), 28040 Madrid, Spain

^b Instituto Universitario de Investigación en Neuroquímica (IUIIN), Universidad Complutense de Madrid (UCM), 28040 Madrid, Spain

^c Departamento de Toxicología y Farmacología, Facultad de Veterinaria, Universidad Complutense de Madrid, 28040 Madrid, Spain

^d Department of Pharmaceutical Chemistry, School of Pharmacy, Aristotle University of Thessaloniki, Thessaloniki 54124, Greece

^e SEPCO (IQOG, CSIC), Juan de la Cierva, 3, 28006 Madrid, Spain

^f Laboratorio de Química Médica (IQOG, CSIC), C/ Juan de la Cierva 3, 28006 Madrid, Spain

^g Department of Chemistry, Centre of Advanced Study, Faculty of Science, Banaras Hindu University, Varanasi 221 005, India

ARTICLE INFO

Article history:

Received 3 September 2013

Received in revised form

9 December 2013

Accepted 19 December 2013

Available online 8 January 2014

Keywords:

11-Amino-12-aryl-8,9,10,12-tetrahydro-7H-chromeno[2,3-b]quinolin-3-ols

Tacrine analogs

Toxicity

EeAChE

hBuChE

Kinetic analysis

Inhibition mechanism

Antioxidant

Neuroprotection

Molecular modeling

ADMET

Alzheimer's disease

ABSTRACT

The pharmacological analysis of racemic chromenotacrines (CT) 1–7, bearing the 11-amino-12-aryl-8,9,10,12-tetrahydro-7H-chromeno[2,3-b]quinolin-3-ol ring skeleton, in a series of experiments targeted to explore their potential use for the treatment of Alzheimer's disease (AD), is reported. The toxicological evaluation showed that among all these chromenotacrines, CT6 is much less hepatotoxic than tacrine in a range of concentrations from 1 to 300 μ M, measured as cell viability in HepG2 cells. Moreover, CT6 did not significantly increase lactate dehydrogenase, aspartate transaminase, and alanine transaminase release in HepG2 cells. Besides, CT6 treatment exerts a high protective effect against the lipid peroxidation induced after H₂O₂-treated SH-SY5Y cells, in a concentration-dependent manner. CT6 showed an excellent antioxidant profile in the AAPH test, and protects against the decrease in cell viability induced by respiratory chain inhibitors (Oligomycin A/Rotenone) and NO donors in neuronal cultures. This effect could be due to a mixed antiapoptotic and antinecrotic neuroprotective effect at low and intermediate CT6 concentrations, respectively. CT1–7 are potent and selective inhibitors of EeAChE in the submicromolar range. CT3 [IC₅₀ (EeAChE) = 0.007 \pm 0.003 μ M], and CT6 [IC₅₀ (EeAChE) = 0.041 \pm 0.001 μ M] are the most potent AChE inhibitors. Kinetic studies on the non-toxic chromenotacrine CT6 showed that this compound behaves as a non-competitive inhibitor (K_i = 0.047 \pm 0.003 μ M), indicating that CT6 binds at the peripheral anionic site, a fact confirmed by molecular modeling analysis. *In silico* ADMET analysis showed also that CT6 should have a moderate BBB permeability. Consequently, non-toxic chromenotacrine CT6 can be considered as an attractive multipotent molecule for the potential treatment of AD.

© 2014 Elsevier Masson SAS. All rights reserved.

Abbreviations: ACh, acetylcholinesterase; AChEI, acetylcholinesterase inhibitor; AD, Alzheimer's disease; ADMET, absorption, distribution, metabolism, excretion, and toxicity; BBB, blood–brain barrier; CSF, cerebrospinal fluid; CNS, central nervous system; CT, chromenotacrine; HIA, human intestinal absorption; log P, calculated logarithm of the octanol/water partition coefficient; MTDL, multi-target-directed-ligand approach; MW, molecular weight; RB, rotatable bond; ROS, radical oxygenated species; TPSA, topological polar surface area.

* Corresponding author. Departamento de Bioquímica y Biología Molecular II, Facultad de Farmacia, Universidad Complutense de Madrid (UCM), 28040 Madrid, Spain. Fax: +34 91 3941779.

** Corresponding author. Laboratorio de Química Médica (IQOG, CSIC), C/Juan de la Cierva 3, 28006 Madrid, Spain. Fax: +34 91 5644853.

*** Corresponding author. Department of Chemistry, Centre of Advanced Study, Faculty of Science, Banaras Hindu University, Varanasi 221 005, India. Fax: +91 542 2368127.

E-mail addresses: mjaset@ucm.es (M.J. Oset-Gasque), knsinghbhu@yahoo.co.in (K.N. Singh), iqoc21@iqog.csic.es (J. Marco-Contelles).

1. Introduction

Alzheimer's disease (AD) is an age-related neurodegenerative process characterized by diverse cognitive impairments [1]. Although the etiology of AD is not yet understood, several factors such as amyloid- β ($A\beta$) deposits [2], τ -protein aggregation, and deficits of acetylcholine (ACh) play significant roles [3]. The cholinergic theory suggests that the selective loss of cholinergic neurons in AD results in low levels of ACh in specific regions of the brain that mediate learning and memory functions [4]. Acetylcholinesterase inhibitors (AChEI), such as tacrine [5], donepezil, rivastigmine, and galanthamine, are well known to improve AD symptoms by inhibiting AChE rising the levels of ACh in the synaptic cleft. Accordingly, these molecules have been approved for commercial use, but with limited success [6], mainly due to the multifactorial nature of AD [7,8].

New therapeutic strategies, such as the Multi-Target-Directed-Ligand approach (MTDL) [9–13], are sought. In this context, some years ago we embarked in a project targeted at the synthesis of a series of multipotent compounds designed to target AChE inhibition and neuronal Ca^{2+} modulation [14]. Thus, we have synthesized and evaluated a number of pyridotacrine (I) and pyranotacrine (II) derivatives, which combine the tetrahydroaminoquinoline moiety present in tacrine with a pyridine or a 4H-pyran ring system (Fig. 1), respectively, a substitution pattern similar to that found in the isosteric 1,4-dihydropyridines [15]. In general, compounds of type I and II were less potent as AChEIs

than tacrine, but they blocked voltage-dependent Ca^{2+} channels [15].

With these precedents, and in order to validate the proposed binding mode, modify the structure of the previous active compounds, and looking for more equipotent AChE vs BuChE inhibitory activities, and increased antioxidant capacities, we reported the synthesis, the biological evaluation, and molecular modeling of a number of racemic β -naphthotacrines (III) bearing the 14-aryl-10,11,12,14-tetrahydro-9H-benzo [5,6]chromeno[2,3-b]quinolin-13-amine ring skeleton (Fig. 1) [16]. From this work, compound 4-(13-amino-10,11,12,14-tetrahydro-9H-benzo [5,6]chromeno[2,3-b]quinolin-14-yl)phenol emerged as a selective, potent and mixed type EeAChE (*Electrophorus electricus* acetylcholinesterase) inhibitor ($IC_{50} = 7 \pm 2$ nM), 4-fold more active than tacrine, but unable to displace propidium iodide, suggesting that the inhibitor does not strongly bind to the PAS of AChE, an observation confirmed later by docking, molecular dynamic simulations, and MM-GBSA calculations [16]. More recently, and based on these results, we have described the synthesis and pharmacological evaluation of a number of racemic, isomeric α -naphthotacrines (IV) bearing the 7-aryl-9,10,11,12-tetrahydro-7H-benzo [7,8]chromeno[2,3-b]quinolin-8-amine structure (Fig. 1) [17]. We hypothesized that changing the location of the fused benzene ring A, on going from compounds of type III to IV, should have consequences in the binding and, consequently, in the AChE inhibition power. From this research we identified 4-(8-amino-9,10,11,12-tetrahydro-7H-benzo [7,8]chromeno[2,3-b]quinolin-7-yl)-2-methoxyphenol as a very potent and selective hAChE (human acetylcholinesterase) inhibitor ($IC_{50} = 0.33 \pm 0.04$ μ M) with antioxidant capacity (1.5 \pm 0.1 Trolox equivalents) [17].

Now, in this context and in the present work, we have focussed our interest in the related 12-aryl-8,9,10,12-tetrahydro-7H-chromeno[2,3-b]quinolin-11-amines (V) [18] (Fig. 1), and report here the toxicological analysis on hepatoma cells, and the inhibition of EeAChE/hBuChE by a series of selected compounds from this family such as the chromenotacrines CT1-7 (Fig. 2). From this study we have identified chromenotacrine 11-amino-12-(3,4,5-trimethoxyphenyl)-8,9,10,12-tetrahydro-7H-chromeno[2,3-b]quinolin-3-ol (CT6) (Fig. 2), as non-toxic in human liver cells, potent and selective EeAChE inhibitor showing antioxidant and neuro-protective properties.

2. Results and discussion

2.1. Chemistry

Racemic CT1-7 (Fig. 2) has been previously synthesized by one of us by Friedländer-type reaction of 2-amino-3-cyano-4H-chromenes and cyclohexanone in the presence of aluminum chloride, under controlled microwave irradiation [18]. CT1-5 and 7 bear different type of substituents at C4' in the aromatic ring at C12, while CT6 is a polysubstituted derivative with the three methoxy groups located at C3', C4' and C5'.

The pyranopyridine ring motif embedded in CT1-7 is present in a number of heterocyclic compounds showing anti-allergic, anti-inflammatory, and estrogenic activities [19]. Among the different substitution patterns known, benzopyrano[2,3-b]pyridines are known to exhibit anti-proliferative [20], cancer chemopreventive [21], anti-bacterial [22], antitumor [23], anti-histaminic [24], and hypotensive [25] activities, but to the best of our knowledge their potential as tacrine analogs for AD has never been addressed. Consequently, and based on the easy availability of molecules of this type, we selected chromenotacrines CT1-7 (Fig. 2) to investigate their pharmacological profile starting with the toxicological and cholinergic properties.

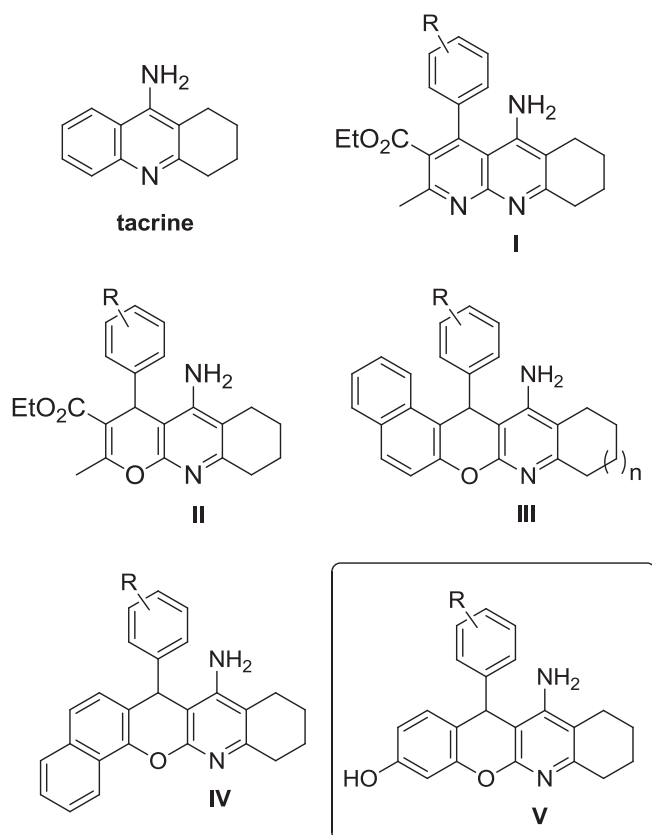


Fig. 1. Structures of tacrine, pyridotacrines (I) and pyranotacrines (II), developed in Macro-Contelles' laboratory [14,15]; tacrine analogs bearing the 14-aryl-10,11,12,14-tetrahydro-9H-benzo [5,6]chromeno[2,3-b]quinolin-13-amine (III) [16], and 7-aryl-9,10,11,12-tetrahydro-7H-benzo [7,8]chromeno[2,3-b]quinolin-8-amine (IV) [17] ring skeletons, and the 12-aryl-8,9,10,12-tetrahydro-7H-chromeno[2,3-b]quinolin-11-amines (V) described in this work.

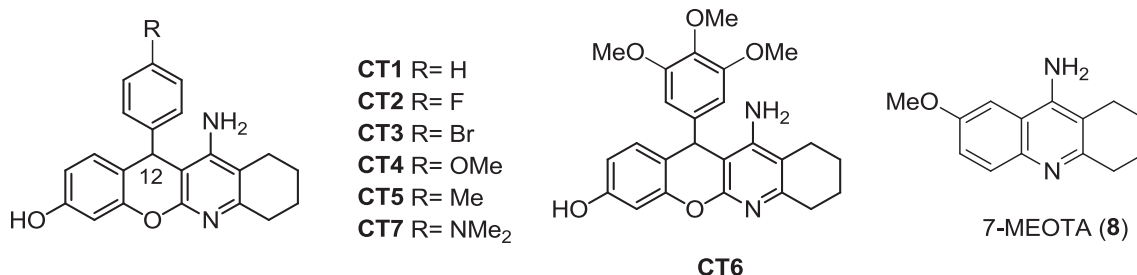


Fig. 2. Structure of the chromenotacrines **CT1–7** analyzed in this work, and 7-METO (**8**).

2.2. Pharmacology and Biochemistry

2.2.1. Toxicological studies of **CT1–7**

The human hepatoma cell line HepG2 is the best-characterized and most frequently used cell line respect to hepatotoxic endpoints and has been used to test metabolism and liver toxicity of several drugs [26]. The evaluation results, using tacrine [27] as a reference compound, are summarized in Table 1. After a 24 h incubation period, at increasing concentrations of each compound tested (1–300 μ M), a decreased concentration dependent pattern was observed in the cell viability. Very interestingly, **CT6** was not toxic at any concentration assayed. The presence of three methoxy groups in the aromatic ring at C12, makes **CT6** a very potent electron-donor polysubstituted, non-toxic chromenotacrine, a fact that clearly confirms that the non-toxic effects of tacrine analogs are associated to the substitution with a methoxy electron-donor substituent, as it is the case of non-toxic tacrine analog 7-MEOTA (**8**) [28] (Fig. 2). Not surprisingly, **CT7** and **CT4**, in this order, bearing the good *N*-dimethylamino and methoxy electron-donor groups, respectively at C4' position, were the less toxic chromenotacrines investigated here. Finally, note that electron-withdrawing substituted chromenotacrines at C4', such as **CT3**, bearing a bromine atom at this position, show less potent cell-viability activity power.

On the other hand, it is known that tacrine has a limited therapeutic window due to the hepatotoxicity associated with the release of aminotransferases [29] and lactate dehydrogenase (LDH) from liver [30]. In order to determine aspartate aminotransferase (AST), alanine aminotransferase (ALT) and LDH levels, we incubated the less toxic chromenotacrine **CT6** and tacrine in HepG2 cells for 24 h. The effects of **CT6** at the three concentrations on these enzymes were not significant, except at the dose of 100 μ M (Table 2). However, tacrine induced a statistically significant increase of ALT and AST at 30 and 100 μ M respect to control group.

Furthermore, we carried out the LDH test (Fig. 3), and compound **CT6** did not show LDH release at any concentration assayed,

whereas tacrine treatment significantly increased cell death in a concentration-dependent manner. This biochemical test in HepG2 proves that **CT6** is less hepatotoxic than tacrine, as showed in the cell viability study.

2.2.2. AChE/BuChE inhibitory activity

CT1–7 were evaluated as inhibitors of *Ee*AChE and horse serum BuChE according to Ellman's protocol [31]. The observed IC₅₀ values for *Ee*AChE inhibition are shown in Table 3.

As shown, **CT1–7** are potent *Ee*AChE inhibitors (Table 3), in the low micromolar range, and very selective, as no inhibition was observed for eqBuChE. The most potent chromenotacrine corresponded to toxic **CT3** (IC₅₀ = 0.007 \pm 0.003 μ M), but the non-toxic **CT6** also showed a good AChE inhibitory profile (IC₅₀ = 0.041 \pm 0.001). However, from the structure–activity relationship perspective, no clear trends could be withdrawn from these data. Particularly interesting is the observed effect of a fluorine atom at C4' compared with bromine at the same position, as **CT2** is 14.7-fold less active than **CT3**. Similarly, **CT5**, bearing a modest methyl electron-donor group, is 8.1-fold more active than **CT4**, bearing only one methoxy group, and in the same range that

Table 2

Aspartate aminotransferase (AST) and alanine aminotransferase (ALT) levels in HepG2 cells treated with **CT6** and tacrine.

Compounds (μ M)	AST (IU/L)	ALT (IU/L)
Control	50.3 \pm 2.90	11.7 \pm 0.88
Tacrine (10)	60.3 \pm 4.10 ^{ns}	12.7 \pm 0.89 ^{ns}
Tacrine (30)	83.3 \pm 3.18 ^{**}	42.7 \pm 3.93 ^{***}
Tacrine (100)	118.7 \pm 8.41 ^{***}	68.3 \pm 1.76 ^{***}
CT6 (10)	53.0 \pm 2.64 ^{ns}	13.0 \pm 2.00 ^{ns}
CT6 (30)	66.0 \pm 2.52 ^{ns}	16.7 \pm 1.86 ^{ns}
CT6 (100)	78.3 \pm 2.40 ^{**}	20.3 \pm 2.33 ^{ns}

Data are expressed as the means \pm SEM of four independent experiments of different cultures. All compounds were assayed at increasing concentrations (10, 30 and 300 μ M). ^{***}*P* < 0.01, ^{**}*P* < 0.01, ns non significant, with respect to control. Statistical analysis: one-way ANOVA followed by the Newman–Keuls post-hoc test.

Table 1

In vitro toxicity of compounds **C1–7** and tacrine, in HepG2 cells.

CT	Viability (%) HepG2 cells					
	1 μ M	3 μ M	10 μ M	30 μ M	100 μ M	300 μ M
1	99.5 \pm 1.49 ^{ns}	67.4 \pm 3.59 ^{***}	66.2 \pm 2.04 ^{***}	62.4 \pm 1.41 ^{***}	55.8 \pm 2.29 ^{***}	49.6 \pm 3.58 ^{***}
2	91 \pm 4.00 ^{ns}	75.1 \pm 4.49 ^{**}	62.8 \pm 3.45 ^{***}	55.7 \pm 1.81 ^{***}	55.5 \pm 2.02 ^{***}	50.1 \pm 3.22 ^{***}
3	99 \pm 3.51 ^{ns}	87.4 \pm 2.05 ^{ns}	84.8 \pm 2.60 [*]	76.9 \pm 2.06 ^{***}	74.4 \pm 2.86 ^{***}	61.5 \pm 1.99 ^{***}
4	97.3 \pm 5.03 ^{ns}	96.8 \pm 3.98 ^{ns}	94.1 \pm 3.37 ^{ns}	95 \pm 1.63 ^{ns}	85.9 \pm 2.44 ^{ns}	75.5 \pm 2.97 ^{**}
5	96.9 \pm 2.55 ^{ns}	89.48 \pm 4.55 ^{ns}	85.6 \pm 1.83 ^{ns}	74.3 \pm 2.26 ^{**}	71.7 \pm 3.35 ^{**}	47.9 \pm 3.88 ^{***}
6	101.9 \pm 1.42^{ns}	98.7 \pm 1.09^{ns}	100.7 \pm 0.66^{ns}	100.4 \pm 0.99^{ns}	98.3 \pm 0.68^{ns}	102.6 \pm 0.68^{ns}
7	99 \pm 0.48 ^{ns}	88.5 \pm 3.22 [*]	86.1 \pm 2.37 [*]	85.5 \pm 1.60 ^{**}	85.5 \pm 0.82 ^{**}	80.3 \pm 2.44 ^{***}
Tacrine	93.4 \pm 4.69 ^{ns}	90 \pm 2.95 ^{ns}	88.7 \pm 3.42 ^{ns}	81.6 \pm 4.88 [*]	64.3 \pm 4.54 ^{***}	40 \pm 2.20 ^{***}

Data are expressed as the means \pm s.e.m. of quadruplicate cell viability measurements in at least four different cultures. All compounds were assayed at increasing concentrations (1–300 μ M). ^{***}*P* < 0.01, ^{**}*P* < 0.01, ^{*}*P* < 0.05, ns non significant, with respect to control.

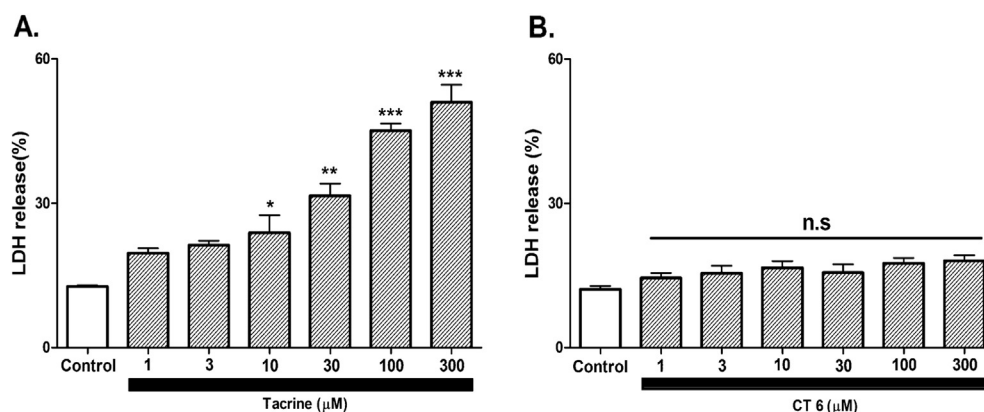


Fig. 3. LDH release in HepG2 cells exposed to compound **CT6** and tacrine. Bars show necrotic cell death, measured as % of LDH release, induced by indicated concentrations of tacrine (A) or CT6 (B). Data represent the mean \pm SEM of four independent experiments in triplicate. n.s (non significant). * $p < 0.05$; ** $p < 0.01$ and *** $p < 0.001$, compared to control.

CT6, bearing three methoxy groups. Finally, note that the parent **CT1** and the methoxy substituted **CT4** showed a very similar inhibition power.

2.2.3. Kinetics of *EeAChE* inhibition by **CT6**

In order to get a deeper insight in the mechanism of the inhibition of these chromenotacrines, the most non-toxic and potent *EeAChE* **CT6** was selected for the analysis of the kinetic of the inhibition.

Graphical analysis of the reciprocal Lineweaver Burk plots (Fig. 4A) showed increased slopes (decreased V_{max}) but not intercepts (similar K_m) at increasing concentration of the inhibitor. This pattern indicates a non-competitive-type inhibition. This was confirmed by statistical analysis of the K_m and V_{max} modifications at different concentrations of **CT6**, which indicate that K_m 's does not significantly change while V_{max} decreased in a statistically significant way in a dose-dependent manner (Table 4). Replots of the $1/V$ versus concentration of **CT6** (Dixon analysis) gave an estimate of the inhibition constant, $K_i = 0.047 \pm 0.003 \mu\text{M}$ (Fig. 4B), a concentration very close to IC_{50} value. These data indicate that **CT6** is bound to the enzyme in a different site than the substrate, such as the peripheral anionic site (PAS) [32]. These results are in good agreement with data deduced from the computational docking analysis (see below Section 2.2.6).

The general structure of **CT6** bearing a phenol group at C3, clearly suggests the possibility that this compound may act as a good radical scavenger, and consequently, able to trap radical oxygenated species (ROS), that are known to play an important role in the progress and development of AD. Accordingly, next, a series of experiments have been designed to analyze this capacity on this chromenotacrine.

Table 3

IC_{50} (μM) values for the inhibition of *Electrophorus electricus* AChE (*EeAChE*) by racemic **CT1-7**.^a

CT	IC_{50} <i>EeAChE</i> (μM)
1	0.55 ± 0.11
2	0.103 ± 0.03
3	0.007 ± 0.003
4	0.53 ± 0.006
5	0.065 ± 0.001
6	0.041 ± 0.001
7	0.29 ± 0.06
Tacrine	0.04 ± 0.002

^a Values are expressed as mean \pm standard error of the mean of at least three different experiments in triplicated.

2.2.4. Antioxidant activity of **CT6**

2.2.4.1. Lipid peroxidation inhibitory effect of **CT6.** Malonyldialdehyde (MDA) is one of the most important intermediates produced during lipid peroxidation. Incubation with H_2O_2 (300 μM) (Fig. 5) in SH-SY5Y cells for 8 h induced a significant increase in MDA levels (8-fold above basal) compared to control group. As shown, **CT6** provided a significant decrease of MDA levels in a concentration-dependent manner.

Lipid peroxidation induced by the water soluble azo compound 2,2'-azobis-2-methyl-propanimidamide dihydrochloride (AAPH) has been used as a clean and controllable source of alkylperoxyl free radicals. In our study, AAPH was used as a free radical initiator to follow oxidative changes of linoleic acid to conjugated diene hydroperoxides. **CT6** showed significant inhibition on lipid peroxidation (LPO) at 100 μM (Table 5) compared to Trolox, used as a standard (63%). Recent findings [33] show that the activation of brain lipoxygenases (LOX) is an early event in the pathogenesis of AD. LOXs play a role in membrane lipid peroxidation by forming hydroperoxides in the lipid bilayer. Inhibition of soybean LOX was performed by the UV absorbance based enzyme assay [34]. Unfortunately, **CT6** showed very low inhibition in comparison to the reference compound nordihydroguaiaretic acid (NDGA).

Next, and in order to know whether **CT6** was able to revert the ROS formation in cortical neurons in culture, two toxic stimuli, sodium nitroprussiate (SNP) and oligomycin-A 10 μM + rotenone 30 μM (OR), were evaluated.

2.2.4.2. Effect of **CT6 on ROS levels in cortical neurons.** As shown in Table 6, SNP (0.5 mM), administered to cortical neurons during 24 h, increased the ROS formation by about 2.5 times respect to control. **CT6** at 10 and 25 μM was able to revert this effect in a 25–40%. These data agree with the weak effect of **CT6** on lipid peroxidation neuroprotection, although in the case of cortical neurons, contrary to the *in vitro* assays, the effects were obtained at lower doses (10–25 μM). At higher **CT6** doses, we observed an increase in the ROS formation, indicating a toxic effect of this compound at these high concentrations.

2.2.5. Neuroprotective effect of **CT6**

Once the ability of **CT6** to scavenge ROS was evaluated, we turned our attention to investigate the capacity of this chromenotacrine to act as a neuroprotectant agent. Thus, we investigated the neuroprotection profile of **CT6** on primary cortical neurons treated with Oligomycin-A (10 μM) and rotenone (30 μM) (OR), two mitochondrial respiratory chain inhibitors, which block complex V

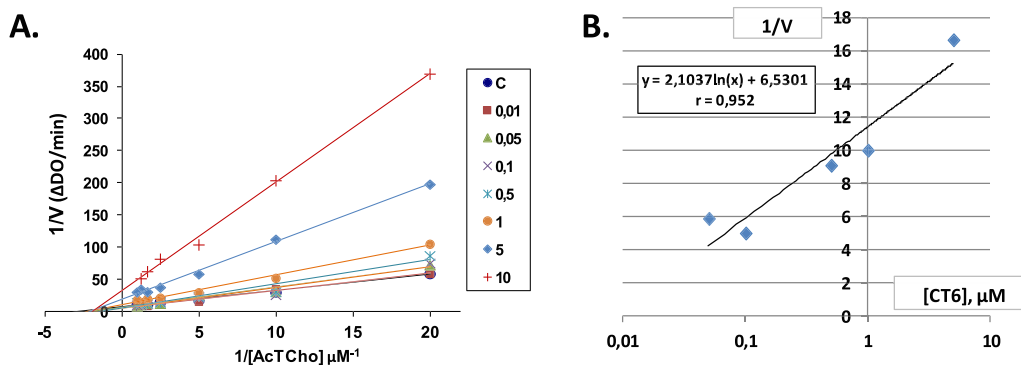


Fig. 4. Kinetics of inhibition of *EeAChE* hydrolysis of acetylthiocholine (ATCh) by **CT6**. (A) Lineweaver–Burk reciprocal plots of initial velocity at substrate concentrations (0.05–10 μM) are presented. Lines were derived from a weighted least-squares analysis of data. (B) K_i calculation for **CT6** by Dixon analysis ($P < 0.001$).

Table 4

Kinetics of the *EeAChE* inhibition for **CT6** (K_m 's and V_{\max} 's).

[CT6], μM	V_{\max} ($\Delta\text{DO}/\text{min}$)	$P <$	K_m (μM)	$P <$
C	0.18 ± 0.056	—	0.46 ± 0.023	—
0.01	0.18 ± 0.033	ns	0.48 ± 0.021	ns
0.05	0.17 ± 0.043	ns	0.54 ± 0.105	ns
0.1	0.20 ± 0.09	ns	0.55 ± 0.068	ns
0.5	0.11 ± 0.008	***	0.54 ± 0.009	ns
1	0.10 ± 0.017	**	0.57 ± 0.019	ns
5	0.05 ± 0.014	***	0.49 ± 0.026	ns
10	0.03 ± 0.005	***	0.53 ± 0.017	ns

Statistical comparisons were carried out against the control (one way ANOVA; $n = 6$). ** $P < 0.01$; *** $P < 0.001$; ns = non significant.

and I respectively, as previously described [35] by using the XTT (2,3-bis(2-methoxy-4-nitro-5-sulfophenyl)-2H-tetrazolyl-5-carboxyanilide) assay to determine neuronal viability.

The **CT6** neuroprotective effect was assayed against the decrease in cell viability induced by both OR and SNP, and was added 15 min before these toxic agents, at concentrations between 0.1 μM and 100 μM . Data in Fig. 6 indicate that **CT6** has a neuroprotective effect against cell death induced by OR (Fig. 6A) and by SNP (Fig. 6B), both conditions producing a decrease in the cellular viability of about a 40%. EC_{50} are very similar, $1.11 \pm 0.07 \mu\text{M}$ and $3.47 \pm 0.81 \mu\text{M}$ for OR and SNP, respectively. However, the highest neuroprotective effects were obtained against SNP-reduced cell viability, since maximal neuroprotective activity was $148.12 \pm 17.63\%$ against SNP but only $81.08 \pm 3.95\%$ against OR. In the case of the OR treatment, a toxic

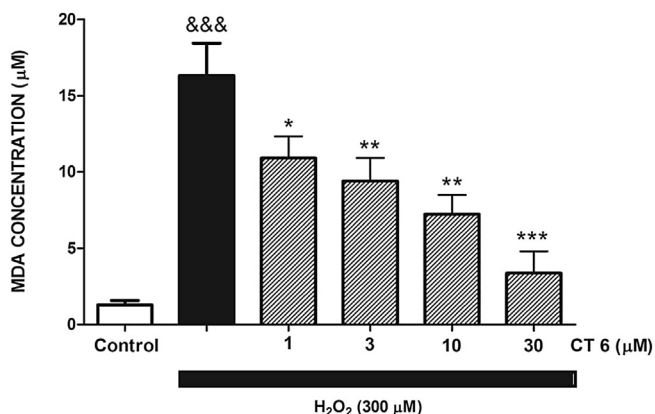


Fig. 5. MDA production in SH-SY5Y cells induced by 300 μM H_2O_2 co-incubated with or without **CT6** (1–30 μM) for 8 h. Data represent the mean \pm s.e.m. of four independent experiments in triplicate. &&& $p < 0.001$ comparing control respect to H_2O_2 . * $p < 0.05$; ** $p < 0.01$ and *** $p < 0.001$ comparing H_2O_2 respect to H_2O_2 plus **CT6**.

Table 5

% Inhibition of lipid peroxidation (AAPH %) and *in vitro* inhibition of soybean lipoyxygenase (LOX %) by **CT6**, Trolox, and NGGA.

Compound	(%) AAPH (100 μM)	(%) LOX Inh. (100 μM)
CT6	85	18
Trolox	63	—
NGGA	—	84

Values are expressed as mean \pm standard error of the mean of at least three different experiments.

effect began at 10–25 μM **CT6**, while in the case of SNP the toxic effect of the drug was only appreciated from 50 μM concentration. The different neuroprotective profile of **CT6** in both cases could be due to the fact that different ROS and RNS could be formed in each case, and to the different ability of **CT6** to scavenge these species in the corresponding oxidative metabolism.

Alternatively, the different neuroprotective effect of **CT6** in the decrease in cell viability induced by OR and SNP could be explained by the cell death type. Thus, while SNP induces both necrosis and apoptosis, OR induces mainly apoptosis at the used doses. In our hands **CT6** was able to completely abolish the apoptosis induced by OR (10 $\mu\text{M}/30 \mu\text{M}$) (1.83 ± 0.08 -fold the control values), while its capacity to reduce 50% of the necrosis induced by 1 mM SNP (3.43 ± 0.41 -fold the control values) requires higher concentrations of at least 25–50 μM . In conclusion, the neuroprotective effect of **CT6** could be antiapoptotic at low concentration and antinecrotic at higher concentrations. However, doses higher than 50 μM seem to be neurotoxic for neurons. These effects are in accordance with the decrease in lipid peroxidation induced by **CT6**.

Table 6

Action of **CT6** on SNP-induced ROS formation in cortical neurons.^a

CT6 [μM]	ROS (ratio over C)
Control	1 ± 0.12
SNP (0.5 mM)	$2.65 \pm 0.46^{***}$
1	$2.31 \pm 0.34^{***ns}$
10	$1.93 \pm 0.38^{***\circ\circ}$
25	$1.81 \pm 0.25^{***\circ\circ\circ}$

^a Cortical neuron cultures were challenged with 0.5 mM SNP during 24 h and ROS levels (H_2O_2) measured as indicated in Material and Methods. Data are expressed as ratios over control and are means \pm SEM of two experiments from different cell cultures, each one performed in triplicate. Statistical comparisons were performed against control (***) or SNP ($\circ\circ\circ$) by one-way ANOVA. *** = $p < 0.001$, ns = non significant.

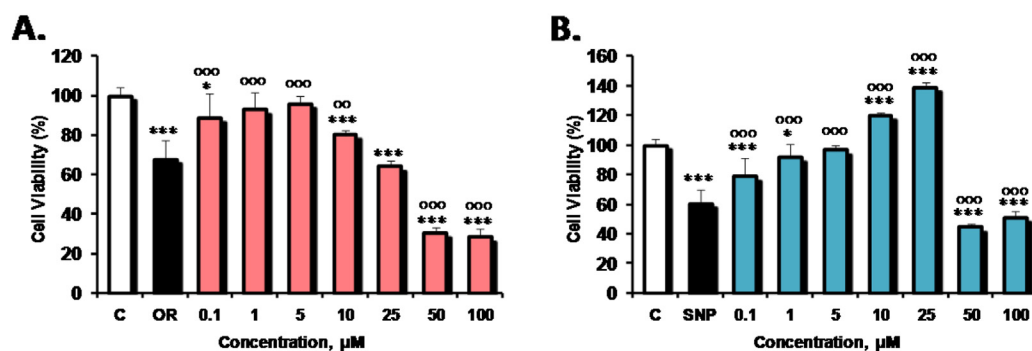


Fig. 6. Neuroprotective effects of **CT6** based on the decrease in cellular viability induced by mitochondrial chain blockers OligA10 μM /Rot 30 μM (A) or 0.5 mM SNP (B) in primary cultures of cortical neurons. The values are the mean \pm SEM of three independent experiments, each one carried out in triplicate, in different cell cultures. The statistical analysis compares the differences against O/R or SNP, in the absence of drugs, (***) or against controls (°°°) at * = $P < 0.05$, ** = $P < 0.01$, *** = $P < 0.001$ (one way ANOVA).

2.2.6. Molecular modeling of CT6

To shed some light on the suitability of the designed compounds shown in Fig. 2 to act as AChE inhibitors, we have performed docking simulations of the (R)- and (S)-enantiomers for compounds **CT6** and **CT3**.

As protein target, the crystallographic structure of the AChE of the electrophorus electricus (PDB: 1C2B) has been selected [36]. Attempts to dock the ligands in the catalytic site of AChE were unsuccessful which pointed out that the catalytic site of AChE is not flexible enough to easily accommodate these bulky compounds. In contrast, the most favored binding mode accommodates the enantiomers (R) of both ligands in the opening of the PAS, located at the rim of the gorge. Thus, the chromenotacrine moiety stacks against Trp286, Phe297 and Tyr72 residues (for **CT6**, see Fig. 7; for **CT3**, see Supplementary material). The tetracyclic skeleton is engaged in hydrophobic interactions with the aromatic residue Tyr124, and with Phe299, Val300 and Leu289. A close examination reveals that the pyridinic N is doubly hydrogen bonded to the Ser298 side chain and backbone, whereas the hydroxylic substituent can establish a hydrogen bond with the backbone of Trp286. The amino group can be probably engaged in a H-bond with

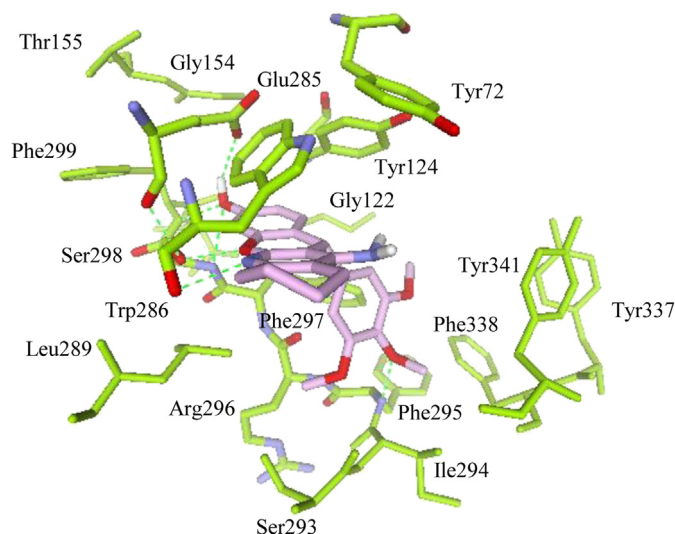


Fig. 8. Putative binding mode of inhibitor (S)-**CT6** at the *EeAChE* gorge predicted by the docking simulation. The ligand is rendered as thick with carbon atoms in pink. Selected residues of the protein are displayed in green (the most relevant residues Trp286, Tyr72, Tyr124, Glu285, Phe295, Arg296, Phe297 and Ser298 are shown as sticks colored according to atoms, carbon atoms in green; other residues are shown as thin sticks in green). Hydrogen-bond interactions are shown by dashed lines.

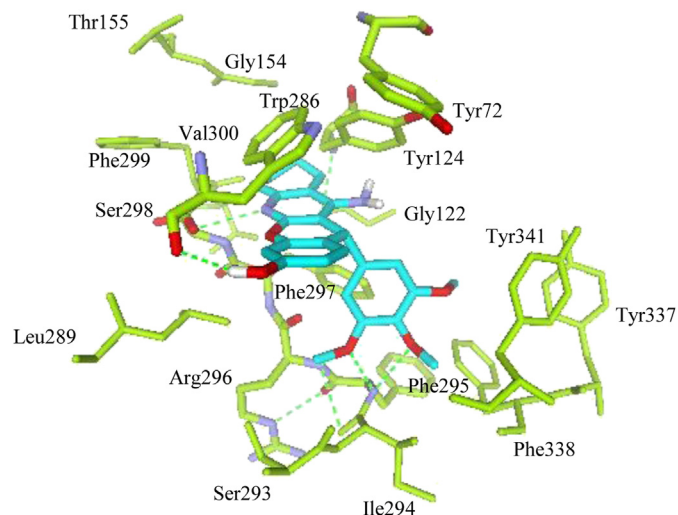


Fig. 7. Putative binding mode of inhibitor (R)-**CT6** at the *EeAChE* gorge predicted by the docking simulation. The ligand is rendered as thick with carbon atoms in cyan. Selected residues of the protein are displayed in green (the most relevant residues Trp286, Tyr72, Tyr124, Phe295, Arg296, Phe297 and Ser298 are shown as sticks colored according to atoms, carbon atoms in green; other residues are shown as thin sticks in green). Hydrogen-bond interactions are shown by dashed lines.

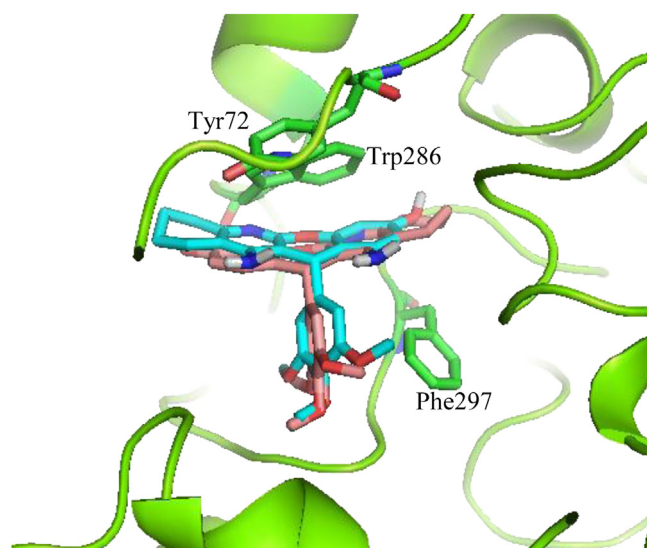


Fig. 9. Superposition of enantiomers of **CT6** in the putative binding site [(R)- in cyan, (S)- in pink].

Table 7
Calculated physicochemical properties for chromenetacrines **CT1–7**.

	CT1	CT2	CT3	CT4	CT5	CT6	CT7	tacrine
Molecular weight	344.41	362.4	378.85	374.43	358.43	434.48	387.47	198.26
No. of H-bond donors	3	3	3	3	3	3	3	2
No. of H-bond acceptor	4	4	4	5	4	7	5	2
No. of Rotatable Bonds	1	1	1	2	1	4	2	0
No. violations Lipinski's rule	0	0	0	0	0	0	0	0
Log <i>P</i> (Moriguchi) ^a	3.61	3.72	3.83	3.04	3.83	1.93	3.25	2.21
Log <i>P</i> ^b	4.28	4.46	4.84	4.18	4.67	3.83	4.34	2.72
TPSA (Å ²)	68.37	68.37	68.37	77.61	68.37	96.06	71.61	38.91
Fraction unbound in plasma	0.04	0.05	0.02	0.04	0.04	0.05	0.03	0.13
Log BB ^{a,c}	0.66	0.57	0.59	0.54	0.63	0.27	0.46	0.30
Log BB ^{b,c}	−0.01	0.04	0.15	0.04	0.18	−0.03	0.13	0.21
Log PS ^d	−1.9	−1.9	−1.7	−2.0	−1.8	−2.3	−2.0	−2.00
Log PB ^d	−0.01	0.04	0.15	0.04	0.18	−0.03	0.09	0.21
Log (PS*fu, brain) ^d	−3.3	−3.3	−3.4	−3.4	−3.4	−3.6	−3.5	−2.9
Human intestinal absorption (%)	94.80	94.81	95.42	94.93	94.94	95.36	95.21	96.52
In vitro Caco-2 perm (nm/sec)	23.27	22.82	21.64	25.64	23.69	26.20	33.24	25.86
Toxicity ^{a,e}	Hepatotoxicity	Hepatotoxicity			Hepatotoxicity			Acute toxicity in rats, hepatotoxicity

^a AMET Predictor, v.6.5.

^b ACD/Percepta 14.0.

^c According to the classification made by Ma et al. [45]: High absorption to CNS: log BB more than 0.3; Middle absorption to CNS: log BB 0.3–1.0; Low absorption to CNS: log BB less than −1.0.

^d Other estimated parameters related to brain penetration were used to classify the compounds as CNS permeable or non-permeable [49]: rate of brain penetration (Log PS) is the rate of passive diffusion/permeability; brain/plasma equilibration rate (Log(PS*fu, brain)); fu, brain – fraction unbound in plasma.

^e Hepatotoxicity is indicated if alkaline phosphatase level is predicted as elevated.

Gly122. The phenyl group is extended to the central region of the gorge forming π – π T-shaped interactions with Phe297; in this orientation, two of the methoxy substituents of **CT6** are involved in H-bond interactions with the backbone of Phe295 and Arg296. In the case of **CT3**, an H-bond is also detected between Br and Phe295 backbone. Additionally, hydrophobic interactions with the aromatic side chains of Phe295, Tyr337, Phe338 and Tyr341 are observed for both (*R*)-ligands, along with Ser293 and Ile294. To note that no interactions with the catalytic triad residues Ser203, Glu334 and His447 have been found.

On other hand, most favorable docking pose for the (*S*)-enantiomer of **CT6** and **CT3** was also found at the PAS (see Fig. 8, and Supplementary material for **CT3**). Binding of (*S*)-enantiomer appears to be as favorable as the (*R*)-enantiomer (binding energy differs just by 0.2 and 0.1 kcal/mol for **CT6** and **CT3**, respectively) because a highly equivalent orientation and mode are observed. Thus, the inhibitor is stacked against Trp286, Phe297 and Tyr72. The ligand–enzyme interaction would be probably further strengthened by a hydrogen bond between the amino group and the hydroxy group of Tyr72. The tetracyclic core forms hydrophobic interactions with the aromatic residue Tyr124, and with Phe299, Val300 and Leu289. The hydroxylic group is doubly hydrogen bonded to the Glu285 side chain and backbone of Ser298, whereas the endocyclic O atom is also predicted to mediate a hydrogen-bond interaction with the hydroxy group of Ser298. The phenyl group interacts by means of π – π T-shaped interactions with Phe297. The methoxy substituents of **CT6** form H-bonds with the backbone of Phe295 and Arg296, whereas the bromine of **CT3** H-bonds with the backbone of Phe295. Finally, hydrophobic interactions with the aromatic side chains of Phe295, Tyr337, Phe338 and Tyr341, and also with Ser293 and Ile294 could stabilize the complex. Analogously to the (*R*)-enantiomer, no interactions with the catalytic triad residues have been detected.

A superposition of both enantiomers of **CT6** on the binding site in the PAS (Fig. 9; for **CT3** see Supplementary material) shows the highly equivalent binding mode with the *Ee*AChE.

In summary, the most probable binding mode for both enantiomers of both ligands is found at the PAS. The binding energy for

each pair of enantiomers and ligands is very similar, thus supporting the values of inhibitory activity. This putative binding mode was also proposed for tacrine-dihydropyridine hybrids, structures closely related to these chromenetacrines, and previously reported by some of us [37]. The rigid tetracyclic core and the presence of a phenyl substituent on a sp^3 -hybridized carbon as well as the predicted interactions with the rich aromatic residues may obstruct a deeper penetration of the ligand along the gorge to reach the catalytic anionic site. Hence, the docking study strongly suggests a binding mode in the PAS and a non-competitive inhibition mechanism for these chromenetacrines.

On the other hand, the lack of a tryptophan residue mimicking Trp286 in the peripheral site of hBuChE (replaced by Ala277), as well as the replacement of Tyr72 in AChE by Asn68 in hBuChE, could also explain the selectivity on AChE over BuChE of these compounds.

2.2.7. ADMET Analysis of the chromenetacrines

Various well known AChE inhibitors, such as ensaculine, donepezil, propidium, rivastigmine, and tacrine, have shown slight improvement in cognitive and memory disorders. However, these available nitrogen containing AChEI drugs have certain side effects and lesser central nervous system (CNS) permeability. So, the new drugs developed for the treatment of AD should present a better CNS penetration profile and decreased toxic effects. To this end, some relevant ADMET (Absorption, Distribution, Metabolism, Excretion and Toxicity) properties were calculated, with special emphasis on the requirements of CNS. The drugs used for neurological disorder treatment are generally CNS acting drugs, so factors that are important to the success of CNS drugs were analyzed. Computer predictions were performed with ADMET Predictor 6.5 [38] and ACD/Percepta 14.0.0 [39] software packages (see Table 7).

Drugs that penetrate CNS should have lower polar surface areas than other kinds of molecules [40]. In the case of CNS, penetrating drugs are estimated at 60 to 90 Å [41,42]. In our study, all the compounds present a proper value, except **CT6** which shows a high TPSA, slightly above the reference value (96.06 Å²).

All the compounds showed significant drug-like characteristics according to the Lipinski's rule of five [43]. A more rigid rule for CNS drugs [42,44] (MW \leq 450, HB donor \leq 3, HB acceptors \leq 7, log $P \leq$ 5, TPSA \leq 90, and number of rotatable bonds \leq 8) is also satisfied for these **CT**, although **CT6** is slightly outlier due to the high polar surface area.

The blood–brain barrier (BBB) is a separation of circulating blood and cerebrospinal fluid (CSF) in the central nervous system (CNS). Blood–Brain Barrier (BBB) penetration is represented as $BB = [\text{Brain}]/[\text{Blood}]$, where [Brain] and [Blood] are the steady-state concentration of radiolabeled compounds in brain and peripheral blood. Predicting BBB penetration means predicting whether compounds pass across the blood–brain barrier. This is crucial in pharmaceutical sphere because CNS-active compounds must pass across it and CNS-inactive compounds mustn't pass across it in order to avoid of CNS side effects. According to the computed values, these chromenotacrine show a brain penetration profile not high but sufficient for CNS activity, although **CT6** presents the poorer penetration [45,46].

On other hand, a middle Caco-2 cell permeability is suggested for all these chromenotacrine [47], as well as a high percent human intestinal absorption (%HIA) [48]. Finally, the prediction of parameters related to toxicity concluded that **CT1**, **CT2** and **CT5** would probably show hepatotoxicity [49], a prediction that has been confirmed by the experimental results (see Section 2.2.1. Toxicological studies of **CT1-7**).

3. Conclusions

In this work we have investigated several pharmacological issues of the well known chromenotacrine **CT1-7**, targeted for their potential application for the treatment of AD, such as the toxicity on HepG2 cells, ChE inhibition, the antioxidant properties and neuroprotection activities. From all the data obtained, we initially have clearly identified racemic chromenotacrine 11-amino-12-(3,4,5-trimethoxyphenyl)-8,9,10,12-tetrahydro-7H-chromeno[2,3-b]quinolin-3-ol (**CT6**) as a non-toxic, compared with tacrine, showing moderate BBB permeability, and a potent, non-competitive, in the low micromolar range, *EeAChE*, and totally selective since **CT6** does not inhibit hBuChE. Molecular modeling analysis confirmed that chromenotacrine **CT6** is a non-competitive *EeAChE* inhibitor, and that both enantiomers are readily accommodated in the opening of the PAS of the enzyme. Calculations also showed that the binding of the (*S*)-enantiomer appears to be as favorable as the (*R*)-enantiomer, due to a highly equivalent orientation observed. In addition, **CT6** behaves as an antioxidant and neuroprotective agent. To sum up, chromenotacrine 11-amino-12-(3,4,5-trimethoxyphenyl)-8,9,10,12-tetrahydro-7H-chromeno[2,3-b]quinolin-3-ol (**CT6**) can be considered as a very attractive multipotent drug for the potential treatment of AD.

4. Experimental part

4.1. Chemistry

CT1-7 have been prepared as reported [18].

4.2. Pharmacology

4.2.1. Materials

DMEM/F-12 (Ham) Medium by Life Technologies, Fetal calf serum (FCS) were purchased from Sera-Lab (Sussex, England). SNAP. Other chemicals were reactive grade products from Merck (Darmstadt, Germany).

4.2.2. Culture of HepG2 cells and treatment

The human hepatoma cell line HepG2 was cultured in Eagle's minimum essential medium (EMEM) supplemented with 15 nonessential amino acids, 1 mM sodium pyruvate, 10% heat-inactivated fetal bovine serum (FBS), 100 units/mL penicillin, and 100 μ g/mL streptomycin (reagents from Invitrogen, Madrid, Spain). Cultures were seeded into flasks containing supplemented medium and maintained at 37 °C in a humidified atmosphere of 5% CO₂ and 95% air. For assays, HepG2 cells were subcultured in 96-well plates at a seeding density of 1×10^5 cells per well. When the HepG2 cells reached 80% confluence, the medium was replaced with fresh medium containing 1–300 μ M compounds or 0.1% DMSO as a vehicle control.

4.2.3. MTT Assay and cell viability

Cell viability, virtually the mitochondrial activity of living cells, was measured by quantitative colorimetric assay with 3-[4,5-dimethylthiazol-2-yl]-2,5-diphenyl-tetrazolium bromide (MTT) (Sigma Aldrich), as described previously [50]. Briefly, 20 μ L of the MTT labeling reagent, at a final concentration of 0.5 mg/mL, was added to each well at the end of the incubation period and the plate was placed in a humidified incubator at 37 °C with 5% CO₂ and 95% air (v/v) for an additional 2 h period. Then, the insoluble formazan was dissolved with dimethylsulfoxide; colorimetric determination of MTT reduction was measured at 540 nm. Control cells treated with 0.1% DMSO were taken as 100% viability.

4.2.4. Measurement of IC₅₀ with *EeAChE*

IC₅₀'s were determined using 0.036 U/mL of *EeAChE*. Enzymatic activity was evaluated by the Ellman's method [31]. The reaction was performed on multiwell Petri dishes of 48 wells in a total volume of 500 μ L. 0.036 U/mL of enzyme in phosphate buffer 0.1 M pH 8 was incubated for 15 min with different drug concentrations at 37 °C. After that the enzymatic reaction was triggered by the addition of 0.35 mM acetylthiocholine and 0.35 mM 5,5'-DiThiobis-(2-NitroBenzoic acid) (DTNB). Absorbance was measured for 5 min in a spectrophotometer BioTek Power Wave XS at 410 nm.

4.2.5. Kinetic analysis of the *AChE* inhibition by **CT6**

To obtain estimates of the inhibition constant K_i , reciprocal plots of $1/V$ versus $1/[S]$ were constructed at different concentrations of the substrate acetylthiocholine (0.05–1 mM), at different concentrations of **CT6** (range 0.01–10 μ M), by using Ellman's method [31]. $1/V_{max}$ of the reciprocal plots were then plotted against the concentrations of **CT6**, to evaluate K_i data, as described [35]. Data analysis was performed with SigmaPlot 11.0 software (Systat Software, a subsidiary of Cranes Software International Ltd.).

4.2.6. Statistical analysis

Data are shown as mean \pm SEM of results obtained from two or three independent experiments from different cultures each one performed in triplicate. Statistical analyses were performed by one way ANOVA test, as indicated in each case. A p -value of 0.05 was considered statistically significant. Fit curves for K_i determinations were performed with SigmaPlot 11.0 software.

4.2.7. Determination of lipid peroxidation

MDA is a breakdown product of the oxidative degradation of cell membrane lipids and it is generally considered an indicator of lipid peroxidation. We evaluated lipid peroxidation induced by H₂O₂ (300 μ M) with or without **CT6** (1–30 μ M) for an 8 h incubation period. Intracellular MDA production was quantified using a thiobarbituric acid reactive substance (TBARS) assay kit (Cell Biolabs Inc., San Diego, CA). Briefly, 1×10^6 cells per well were seeded in a six-well plate, then collected in 200 μ L of culture medium and

sonicated for 3×5 s intervals at 40V over ice. SDS Lysis solution (100 μ L) was added to the sample solution and the MDA standards in a microcentrifuge tube and mix thoroughly. Then, 250 μ L of TBA reagent were added to each sample and standard to be tested, and incubate at 95 °C for 45–60 min. Each sample and standard (200 μ L) were loaded (in duplicate) into a clear 96-well plate and the absorbance at 532 nm was recorded using a microplate reader (Biochrom ASYS UVM 340, Cambridge, UK). The content of MDA was calculated for each sample from a standard curve.

4.2.8. Inhibition of linoleic acid lipid peroxidation [33]

Production of conjugated diene hydroperoxide by oxidation of linoleic acid in an aqueous dispersion is monitored at 234 nm. AAPH is used as a free radical initiator. Ten microliters of the 16 mM sodium linoleate dispersion was added to the UV cuvette containing 0.93 mL of 0.05 M phosphate buffer, pH 7.4 pre-thermostated at 37 °C. The oxidation reaction was initiated at 37 °C under air by the addition of 50 μ L of 40 mM AAPH solution. Oxidation was carried out in the presence of aliquots (10 mL) in the assay without anti-oxidant, lipid oxidation was measured in the presence of the same level of DMSO. The rate of oxidation at 37 °C was monitored by recording the increase in absorption at 234 nm caused by conjugated diene hydroperoxides.

4.2.9. Soybean lipoxygenase inhibition study in vitro

[33]. Compound **CT6** dissolved in DMSO were incubated at room temperature with sodium linoleate (0.1 mL) and 0.2 mL of enzyme solution ($1/9 \times 10^{-4}$ w/v in saline). The conversion of sodium linoleate to 13-hydroperoxylinoleic acid at 234 nm was recorded and compared with the appropriate standard inhibitor.

4.2.10. Cell isolation and culture

Primary neuronal cultures from rat cerebral cortex were prepared as previously described [35] with minor modifications. All procedures associated with animal experiments were approved by the Ethics Committee of Universidad Complutense de Madrid (UCM), Madrid (Spain). Cell suspensions from cerebral cortex were prepared from 19-day-old Wistar rat embryos. Living cells in cell suspension were counted by trypan blue exclusion method. Cells were seeded on plastic 48 well multidishes, precoated with 0.05 mg/mL poly D-lysine at a density of 2×10^5 cells/well, and were kept at 37 °C in a 5% CO₂ atmosphere in high glucose Dulbecco's medium supplemented with 15% heat-inactivated (56 °C for 30 min) fetal calf serum. After 48 h, cultured cells were placed and maintained in a serum-free medium (Dulbecco's: Ham's F12, 1:1 [vol/vol] containing 3.15 mg/mL glucose, 2.5 mM Glutamax, and 0.5 mM sodium pyruvate (DMEM/F-12, GlutaMAX™; GIBCO, Life Technologies, Madrid (Spain), 1% Antibiotic–Antimycotic (Gibco; Life Technologies, Madrid, Spain) at 100 units of penicillin, 100 μ g of streptomycin, and 0.25 μ g of amphotericin B final concentrations, and supplemented with 1% B27 medium (Gibco; Life Technologies, Madrid (Spain)). Six- to nine day cultures were used in the experiments. Glial contamination was measured following the usual protocol [51]. Under these conditions the glial cells represented $9\% \pm 3\%$ of the total cell population.

4.2.11. Cell viability

It was determined by the XTT method. This assay is based on the ability of living metabolically active cells to reduce the yellow tetrazolium salt (XTT) to form an orange formazan dye. Therefore, the conversion only occurs in living cells. The formazan dye formed is directly quantified using a scanning multiwell spectrophotometer at wavelength 492 nm (reference wavelength 690). The amount of orange formazan formed, as monitored by the absorbance, directly correlates to the number of living cells. Control and

treated neurones were washed with PBS and incubated with the XTT solution (final concentration 0.3 mg/mL) according to the Kit specifications. After this incubation period, orange dye solution was spectrophotometrically quantified. Results are expressed as percentages with respect to the control cells.

4.2.12. Measurement of the ROS formation

To assay the ROS formation, 2,7-dichlorodihydrofluorescein diacetate (H₂DCF-DA), a non-fluorescent lipophilic reagent, was used. H₂DCF-DA enters into the cells, where it is transformed into 2,7-dichlorodihydrofluorescein (H₂DCF) by the action of intracellular esterase. H₂DCF is oxidized to fluorescent DCF by hydrogen peroxide. H₂DCF-DA (5 μ M) was added to the cells, at the moment in which they were subjected to the different treatments. After each treatment the incubation medium was removed and the cells were washed twice with PBS and the fluorescence was measured in an FL600-BioTek spectrofluorometer with filters of 485 nm exc and 530 nm em. Results were expressed as arbitrary fluorescence units (AFU) in percentage respect to control cells.

4.2.13. Assessment of cell viability after exposure of cell cultures to oligomycin-rotenone treatments

To investigate the neuroprotective effect of tacrine and analogous compounds, several concentrations of these compounds between 0.01 and 100 μ M were used. Neuroprotection was assayed by measuring the increase in cell viability after 24 h treatment with a mixture of 30 μ M rotenone and 10 μ M Oligomycin-A, which induced neuronal cell death. The mixture of rotenone plus oligomycin-A blocks mitochondrial electron transport chain complexes I and V, respectively, inducing cell death by oxidative stress.

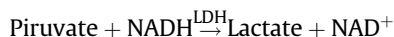
Cell viability, specifically the mitochondrial activity of living cells, was measured by quantitative colorimetric assay with the mitochondrial probe XTT [2,3-bis(2-methoxy-4-nitro-5-sulfo phenyl)-2H-tetrazolium-5-carboxanilide sodium salt] (Roche, Madrid, Spain), based on the ability of living metabolically active cells to reduce the yellow tetrazolium salt (XTT) to form an orange formazan dye, whose quantity directly correlates to the number of living cells. Measurements were carried out on neuronal cell cultures seeded into 48-well culture plates as described [35]. Briefly, control and treated neuronal cultures (2×10^5 cells/well) were incubated with the XTT solution at 0.3 mg/ml final concentration for 3 h in a humidified incubator at 37 °C with 5% CO₂ and 95% air (v/v) and the soluble orange formazan dye formed was spectrophotometrically quantified, using a Biotek PowerWave XS spectrophotometer microplate-reader at 450 nm (reference 650 nm). All XTT assays were performed in triplicate in cells of different batches. Control cells treated with EMEM alone were regarded as 100% viability. Controls containing different DMSO concentrations (0.001–1% DMSO) were performed in all assays.

4.2.14. Determination of hepatic aspartate aminotransferase (AST) and alanine aminotransferase (ALT) levels

The ALT and AST levels were tested as a marker of hepatotoxicity. HepG2 cells were maintained in a 25 cm³ culture flasks and incubated in a humidified incubator at 37 °C with 5% CO₂ and 95% air (v/v). After 48 h, cells were treated with **CT6** and tacrine at different concentrations (10, 30, and 100 μ M). Control cells received 0.1% of DMSO instead of **CT6** or tacrine. After incubation for 24 h, cell supernatants were collected and centrifuged at 1000 g for 5 min at 4 °C. ALA and AST levels were measured with an automatic biochemical analyzer Cobas Integra 400 Plus (Roche, Madrid, Spain). The results were expressed as unit per liter (U/L). One unit of AST and ALT is defined as the amount of enzyme that generates 1.0 μ mol of glutamate and pyruvate respectively per minute at 37 °C.

4.2.15. Lactate dehydrogenase (LDH) release

LDH activity was measured as the rate of decrease in the absorbance at 340 nm, resulting from the oxidation of NADH, according to the following reaction



For the determination of LDH, the culture medium from the control and treated cells was collected. The neurones were homogenized with 0.1 M Tris–HCl (pH 7.4), containing 0.1% Triton X-100. Homogenates were centrifuged at 13,000 g for 10 min. The amount of proteins in cells lysated was monitored by the Bradford technique [51]. LDH activity was measured in the cell supernatants and in the collected culture medium according to [52]. LDH release is given as percentage of LDH release with respect to the total LDH content (LDH in the supernatant + LDH inside the cells).

4.2.16. Caspase-3 activity measurement

Caspase-3 activity was measured as described [53]. Briefly, control and treated cortical neurons were washed rapidly with PBS and homogenized with cell lysis buffer (10 mM Tris–HCl, 10 mM NaH₂PO₄/Na₂HPO₄, pH 7.5, 130 mM NaCl, 0.5% Triton X-100, 10 mM Na₄P₂O₇ and 2 mM DTT). Homogenates were centrifuged at 13,000 g for 5 min. Caspase-3 activity was measured in the supernatants. Supernatants with at least 20 µg of protein were incubated at 37 °C for 2–4 h in caspase-3 assay buffer (20 mM HEPES, pH 7.5, with 2 mM DTT) and 20 µM Ac. DEVD-AMC [*N*-acetyl-Asp-Glu-Val-Asp-(7-amino-4-methylcoumarin)]. The fluorogenic AMC liberated from Ac-DEVD-AMC was monitored using a spectrofluorometer (Bio-Tek FL 600) at an excitation wavelength of 360 nm and an emission wavelength of 460 nm. Under these conditions the emission was linear between, at least, 0–6 h, depending on the caspase-3 activity. Enzymatic activity was expressed as arbitrary fluorescence unit after 1 h per mg protein (AFU/h/mg protein).

4.3. Docking studies

The geometry of the ligands were optimized using the ab initio quantum chemistry program Gaussian 09 and the B3LYP/3-21G* basis set. A set of atom-centered RHF 6-31G* charges was then obtained by using the RESP methodology [54].

The crystallographic structure of the acetylcholinesterase with sequence from *Electrophorus electricus* was retrieved from the Protein Data Bank (PDB code: 1C2B) [36] as target protein. Missing atoms were reconstructed with SwissPDB Viewer 4.1.0 [55].

The docking experiments were carried out using the Lamarckian genetic algorithm implemented in the AutoDock 4.2 program [56]. Two consecutive docking runs were carried out. Initially, a box encompassing the whole protein target was defined with a distance-dependent dielectric constant and a grid spacing of 1 Å for the calculation of energy maps by means of AutoGrid4. The results clearly showed the ligand poses around the PAS. Therefore, a second run was performed on the region of interest at a higher resolution to get more reliable results. A box encompassing both the CAS and the PAS site was defined for the exploration of possible binding modes. A volume for exploration was defined in the shape of a three-dimensional cubic grid (60 × 72 × 60 Å³) at a resolution of 0.3 Å and centered on the gorge that enclosed the residues that are known to make up the inhibitors binding pockets and modes.

At each grid point, the receptor's atomic affinity potentials for carbon, oxygen, nitrogen, and hydrogen atoms present in the ligand were pre-calculated for rapid intra- and intermolecular energy evaluation of the docking solution.

Different conformers of the ligands were docked by randomly changing the torsion angles and overall orientation of the molecule.

The receptor residues Trp286, Tyr124, Tyr337, Tyr72, Asp74, Thr75, Trp86, and Tyr341 were selected to keep flexible during docking simulation with the AutoTors module. The program searched until a maximum of 100 conformations and the procedure was repeated 100 times (runs). After docking, the 100 solutions were clustered in groups with RMSD less than 1.0 Å. The clusters were ranked by the lowest energy representative of each cluster. For all other parameters, the default values were used with AutoDock Tools.

Acknowledgments

JMC thanks MINECO (SAF2012-33304) for support. MJOJG thanks MICINN (SAF2010-20337) and UCM-Santander (GR35/10-B) for financial support.

Appendix A. Supplementary data

Supplementary data related to this article can be found at <http://dx.doi.org/10.1016/j.ejmech.2013.12.021>.

References

- [1] M. Goedert, M.G.A. Spillantini, *Science* 314 (2006) 777–781.
- [2] A. Castro, A. Martínez, *Curr. Pharm. Des.* 12 (2006) 4377–4387.
- [3] J.L. Cummings, *Rev. Neurol. Dis.* 1 (2004) 60–69.
- [4] V.N. Talesa, *Mech. Ageing Dev.* 122 (2001) 1961–1969.
- [5] A. Romero, R. Cacabelos, M.J. Oset-Gasque, A. Samadi, J. Marco-Contelles, *Bioorg. Med. Chem. Lett.* 23 (2013) 1916–1922.
- [6] M. Racchi, M. Mazzucchelli, E. Porrello, C. Lanni, S. Govoni, *Pharmacol. Res.* 50 (2004) 441–451.
- [7] N.C. Inestrosa, A. Álvarez, C.A. Pérez, R.D. Moreno, M. Vicente, C. Linker, O.I. Casanueva, C. Soto, J. Garrido, *Neuron* 16 (1996) 881–891.
- [8] M. Bartolini, C. Bertucci, V. Cavrini, V. Andrisano, *Biochem. Pharmacol.* 65 (2003) 407–416.
- [9] A. Cavalli, M.L. Bolognesi, S. Capsoni, V. Andrisano, M. Bartolini, E. Margotti, A. Cattaneo, M. Recanatini, C. Melchiorre, *Angew. Chem. Int. Ed.* 46 (2007) 3689–3692.
- [10] D. Muñoz-Torrero, P. Camps, *Curr. Med. Chem.* 13 (2006) 399–422.
- [11] L. Savini, A. Gaeta, C. Fattorusso, B. Catalanotti, G. Campiani, L. Chiasserini, C. Pellerano, E. Novellino, D. McKissic, A. Saxena, *J. Med. Chem.* 46 (2003) 1–4.
- [12] P.R. Carlier, E.S. Chow, Y. Han, J. Liu, J. El Yazal, Y.P. Pang, *J. Med. Chem.* 42 (1999) 4225–4231.
- [13] A. Cavalli, M.L. Bolognesi, A. Minarini, M. Rosini, V. Tumiatti, M. Recanatini, C. Melchiorre, *J. Med. Chem.* 51 (2008) 347–372.
- [14] R. León, A.G. García, J. Marco-Contelles, *Med. Res. Rev.* 33 (2013) 139–189.
- [15] R. León, J. Marco-Contelles, *Curr. Med. Chem.* 11 (2011) 552–576.
- [16] E. Maalej, F. Chabchoub, A. Samadi, C. de los Ríos, A. Perona, A. Morreale, J. Marco-Contelles, *Bioorg. Med. Chem.* 21 (2011) 2384–2388.
- [17] E. Maalej, F. Chabchoub, M.J. Oset-Gasque, M. Esquivias-Pérez, M.P. González, L. Monjas, C. de los Ríos, M.I. Rodríguez-Franco, I. Iriepa, I. Moraleda, M. Chioua, A. Romero, J. Marco-Contelles, A. Samadi, *Eur. J. Med. Chem.* 54 (2012) 750–763.
- [18] D.S. Raghuvanshi, K.N. Singh, *ARKIVOC* (2010) 305–317.
- [19] S. Ahmad, *J. Nat. Prod.* 47 (1984) 391–392.
- [20] G. Kolokythas, N. Pouli, P. Marakos, H. Pratsinis, D. Kletsas, *Eur. J. Med. Chem.* 41 (2006) 71–79.
- [21] M.A. Azuine, H. Tokuda, J. Takayasu, F. Enjyo, T. Mukainaka, T. Konoshima, H. Nishino, G. Kapadia, *J. Pharmacol. Res.* 49 (2004) 161–169.
- [22] S.K. Srivastava, R.P. Tripathi, R. Ramachandran, *J. Biol. Chem.* 280 (2005) 30273–30281.
- [23] S. Toshiro, W. Noriko, *Eur. Pat. Appl. EP 647445 A1* 19950412, 1995.
- [24] Y. Ito, H. Kato, S. Yasuda, N. Kato, N. Iwasaki, H. Nishino, M. Takeshita, *Jpn. Kokai Tokkyo Koho, JP 06107664 A2* 19940419, 1994.
- [25] K. Goto, O. Yaoka, T. Oe, *PCT Int. Appl. WO 8401711 A1* 19840510, 1984.
- [26] F. Noor, J. Niklas, U. Müller-Viera, E. Heinzie, *Toxicol. Appl. Pharmacol.* 237 (2009) 221.
- [27] S.I. Gracon, M.J. Knapp, W.G. Berghoff, M. Pierce, R. de Jong, S.J. Lobbstaal, J. Symons, S.L. Dombey, F.A. Luscombe, D. Kraemer, *Alzheimer Dis. Assoc. Disord.* 12 (1998) 93–101.
- [28] J. Fusek, J. Patocka, J. Bajgar, M. Koupilova, V. Hrdina, *Act. Nerv. Super.* 28 (4) (1986) 327–328.
- [29] P.B. Watkins, H.J. Zimmerman, M.J. Knapp, S.I. Gracon, K.W. Lewis, *JAMA* 271 (1994) 992–998.
- [30] M.A. Xiao-Chao, X. Jian, W. Hai-Xue, Z. Ting, T.U. Zeng-Hong, *Acta Pharmacol. Sin.* 24 (2003) 247–250.
- [31] G.L. Ellman, K.D. Courtney, B.J. Andres, R.M. Featherstone, *Biochem. Pharmacol.* 7 (1961) 88–95.

- [32] S.K. Fisher, S. Wonnacott, Acetylcholine, in: S.T. Brady, G.J. Siegel (Eds.), *Basic Neurochemistry. Principles of Molecular, Cellular and Medical Neurobiology*, eighth ed., Elsevier, 2012, pp. 258–282.
- [33] M. Chioua, D. Sucunza, E. Soriano, D. Hadjipavlou-Litina, A. Alcázar, I. Ayuso, M.J. Oset-Gasque, M.P. González, L. Monjas, M.I. Rodríguez-Franco, J. Marco-Contelles, A. Samadi, *J. Med. Chem.* 55 (2012) 153–168.
- [34] Y. Yao, C.M. Clark, J.Q. Trojanowski, V.M.-Y. Lee, D. Praticò, *Ann. Neurol.* 58 (2005) 623–626.
- [35] M. Esquivias-Pérez, E. Maalej, A. Romero, F. Chabchoub, A. Samadi, J. Marco-Contelles, M.J. Oset-Gasque, *Chem. Res. Toxicol.* 26 (2013) 986–992.
- [36] Y. Bourne, J. Grassi, P.E. Bougis, P. Marchot, *J. Biol. Chem.* 274 (1999) 30370–30376.
- [37] R. León, C. de los Ríos, J. Marco-Contelles, O. Huertas, X. Barril, F.J. Luque, M.G. López, A.G. García, M. Villarroya, *Bioorg Med. Chem.* 16 (2008) 7759–7769.
- [38] AMET Predictor, v.6.5, Simulations Plus, Inc., Lancaster, CA, 2013.
- [39] ACD/Percepta 14.0.0, Advanced Chemistry Development, 2013.
- [40] U. Kragh-Hansen, *Pharmacol. Rev.* 33 (1981) 17–22.
- [41] T.T. Wager, R.Y. Chandrasekaran, X. Hou, M.D. Troutman, P.R. Verhoest, A. Villalobos, Y. Will, *ACS Chem. Neurosci.* 1 (2010) 420–434.
- [42] D. Meanwell, *Chem. Res. Toxicol.* 24 (2011) 1420–1456.
- [43] C.A. Lipinski, F. Lombardo, B.W. Dominy, P.J. Feeney, *Adv. Drug. Deliv. Rev.* 46 (2001) 3–26.
- [44] H. Pajouhesh, G.R. Lenz, *NeuroRx* 2 (2005) 541–553.
- [45] X. Ma, C. Chen, J. Yang, *Acta Pharmacol. Sin.* 26 (2005) 500–512.
- [46] The same trend is also suggested by other theoretical models: (a) F. Cheng, W. Li, Y. Zhou, J. Shen, Z. Wu, G. Liu, P.W. Lee, Y. Tang, *J. Chem. Inf. Model* 52 (2012) 3099–3105; (b) PreADMET 2.0, Bioinformatics & Molecular Design Research Center (BMDRC), Yonsei University (Seoul).
- [47] S. Yamashita, T. Furubayashi, M. Kataoka, T. Sakane, H. Sezaki, H. Tokuda, *Eur. J. Pharm. Sci.* 10 (2000) 195–204.
- [48] S. Yee, *Pharm. Res.* 14 (1997) 763–766.
- [49] The details can be found on the FDA website: <http://www.fda.gov>.
- [50] F. Denizot, R. Lang, *J. Immunol. Methods* 89 (1986) 271–277.
- [51] M.A. Bradford, *Anal. Biochem.* 72 (1976) 248–253.
- [52] S. Figueroa, M.J. Oset-Gasque, C. Arce, C. Martínez-Honduvilla, M.P. González, *J. Neurosci. Res.* 83 (2006) 441–449.
- [53] E. López, S. Figueroa, M.J. Oset-Gasque, M.P. González, *Br. J. Pharmacol.* 138 (2003) 901–911.
- [54] A.J. Knox, M.J. Meegan, D.G. Lloyd, *Curr. Top. Med. Chem.* 6 (2006) 217–243.
- [55] SwissPdb Viewer 4.1.0, GlaxoSmithKline R&D, Switzerland, 2012.
- [56] G.M. Morris, R. Huey, W. Lindstrom, M.F. Sanner, R.K. Belew, D.S. Goodsell, A.J. Olson, *J. Comp. Chem.* 16 (2009) 2785–2791.